International Journal of Heat and Mass Transfer 55 (2012) 1076–1082

Contents lists available at SciVerse ScienceDirect

International Journal of Heat and Mass Transfer

journal homepage: www.elsevier.com/locate/ijhmt

Simulation and experimental validation of heat transfer in a novel hybrid solar panel

D.J. Yang *, Z.F. Yuan, P.H. Lee, H.M. Yin

Department of Civil Engineering and Engineering Mechanics, Columbia University, 610 SW Mudd, 500 West 120th Street, New York, NY 10027, United States

ARTICLE INFO

Article history:
Received 18 March 2011
Received in revised form 30 September 2011
Available online 21 October 2011

Keywords:
Finite element method
Functionally graded material
Heat transfer
Hybrid solar panel
Solar energy

ABSTRACT

A hybrid solar panel has been invented to integrate photovoltaic (PV) cells onto a substrate through a functionally graded material (FGM) with water tubes cast inside, through which water serves as both heat sink and solar heat collector. Therefore, the PV cells can work at a relatively low temperature while the heat conduction to the substrate can be minimized. Solar panel prototypes have been fabricated and tested at different water flow rates and solar irradiation intensities. The temperature distribution in the solar panel is measured and simulated to evaluate the performance of the solar panel. The finite element simulation results are very consistent with the experimental data. The understanding of heat transfer in the hybrid solar panel prototypes will provide a foundation for future solar panel design and optimization. The finite element model is general and can be extended for different material design and other size of panels.

1. Introduction

Solar panels have become a very promising and popular approach to collect solar energy. Currently solar panel products in market mainly use photovoltaic (PV) cells for the electricity generation. PV technology has achieved tremendous progress since the invention in 1839. However, there is still significant research need in the aspects of efficiency improvement and life-cycle cost reduction. For the single crystalline single junction Si technology, the conversion efficiency keeps lower than 30% [1,2]. Thus a large portion of solar energy is wasted through heat dissipation [3,4]. Although some emerging technologies can considerably improve energy utilization efficiency, such as multi-junction cells [5], optical frequency shifting [6], multiple exciton generation cells [7], hot carrier cells [8] and concentration photovoltaic system [9], these technologies require high cost and complex service conditions, and thus have not been commercially used in solar roofing panel yet.

Solar thermal technology provides another way to use the thermal energy of solar insolation. Solar thermal collectors have been applied to domestic (bath, cooking, space heating and swimming pool heating etc.) and commercial sectors (pre-heating of boiler and hospitals etc.). Typically, energy payback time (EPBT) for solar thermal system is much less than that of PV systems. The EPBT of PV system can be reduced by using it in a hybrid system integrating PV with solar thermal components, such as hot water (HW) tubes [10]. The combination of the above two approaches is not a simple superposition of the materials and costs, but provides a viable solution to significantly increase overall energy utilization efficiency while alleviating the disadvantages of a single approach [11]. A PV-thermal collector enables heat harvesting while improving the PV utilization efficiency by controlling the temperature of PV modules. Currently, some groups have studied the performance of PV-thermal hybrid systems [12,13], which provide the good justifications of the solar hybrid approaches.

In this work, we developed a novel functionally graded material (FGM) based hybrid solar panel as Fig. 1 [14]. A PV surface layer, transferring the photo energy into electricity, is bonded to a structural substrate plate through a functionally graded material (FGM) interlayer. The FGM contains aluminum powder dispersed in a high density polyethylene (HDPE) matrix with a graded microstructure seen in the left top of Fig. 1. Water pipelines are cast within the FGM to control the panel's temperature. The substrate, namely, plastic lumber made of recycled polymer, provides mechanical loading support and heat insulation of the roof.

FGMs are characterized by continuous variation of the volume fraction of the constituents [15]. FGMs have attracted significant interests among researchers and engineers because of their unique thermo-mechanical properties and microstructures [16–18]. The effective material properties, such as thermal conductivity, vary continuously in the gradation direction and keep constant in the plane normal to the gradation direction [16]. In the following experiment, the Al powder concentration gradually decreases from the top to the bottom. Thus the thermal conductivity also decreases gradually from the top to the bottom of the FGM layer.

The remainder of this paper is organized as follows: Section 2 introduces the hybrid solar panel prototype fabrication, and testing instruments and procedure. In Section 3, the irradiation space

* Corresponding author. Tel.: +1 347 371 2259; fax: +1 212 854 6267.
E-mail address: dy2209@columbia.edu (D.J. Yang).

0017-9310/$ - see front matter © 2011 Elsevier Ltd. All rights reserved.
doi:10.1016/j.ijheatmasstransfer.2011.10.003

Nomenclature

C	specific heat	K	thermal conductivity
D	copper tube diameter	m	mass of water
E_{in}	input solar energy	Nu	Nusselt number
E_{rad}	radiation heat loss	s	Stefan–Boltzmann Constant
E_{con}	convection heat loss	T_{pv}	PV cell temperature
E_{pv}	PV cell energy	T_{am}	ambient temperature
E_{water}	thermal energy from water	V_{ac}	open circuit voltage
h_c	convection coefficient of air	η_{pv}	PV cell efficiency
h_w	convection coefficient of water	ϕ	volume fraction
I_{sc}	short circuit current	ΔT	temperature difference
$\bar{k}$	effective thermal conductivity	ε	surface emissivity of silicon

uniformity of the metal halide lamp and the temperature distribution of the solar panel are characterized. A finite element model (FEM) is implemented using ABAQUS to simulate the thermal transfer characteristics of the solar panel. The FEM results are compared with the experimental data. The overall energy efficiency of the solar panel is evaluated based on the testing results. Finally, some conclusions are drawn in Section 4.

2. Experimental set up and procedure

2.1. Solar panel fabrication

The hybrid solar panel has been fabricated for photovoltaic (PV), hot water utilization through a multilayered configuration. The PV cells used in the panels are commercial single crystalline Si solar cells with an open circuit voltage V_{oc} of 0.55 V, short circuit current I_{sc} of 4400 mA and an energy conversion efficiency $_{pv}$ of 13% at room temperature (25 °C). The length, width and thickness of the solar cell are 12.5 cm, 12.5 cm and 270 m, respectively. Pure Al powder and high density polyethylene (HDPE) matrix are used to fabricate the FGM layer. The thermal conductivity of Al and HDPE are 238 and 0.26 W/m K, respectively. The HDPE and Al powder are mixed layer by layer with a continuously changing proportion such as 50% Al volume fraction in the bottom and pure HDPE in the top of a mold. The mix within the mold is baked in a vacuum at 200 °C for 1.5 h and is then solidified with dimensions of 30.5 × 30.5 × 1.5 cm. A vacuum sintering process is employed to bond the FGM layer with the plastic lumber substrate which is made of recycled polymeric materials. The water tubes made with copper (Cu) pipes with a diameter of ~6 mm are cast into the FGM layer with a separation of 2.5 cm. Thermal conductive paste with a conductivity of 1.9 W/m K is used as an adhesive between the PV, and FGM layers. The complete panels are degassed in a vacuum oven at 90 °C for 2 h.

The photovoltaic (PV) layer can transfer a portion of the solar energy to electricity. The thin PV layer improves the heat conduction and structural integrity within the panel, and protects the polymer materials underneath from UV radiation. The high percentage of aluminum (Al) powder in top surface of the FGM makes rapidly heat transfer into the water tubes, but below them the heat conduction is blocked by the HDPE and the plastic lumber substrate. The hot water, whose temperature is partially controlled by the flow rate, can be directly utilized by water heating systems for domestic usage.

2.2. Testing method

Eight T type thermal couples (±1 °C) are attached on the panels to detect the temperature distribution of the PV cells and water. The solar panels are tested in a solar room equipped with a metal halide lamp, which can provide irradiation up to 4 KW/m^2. The panel is fixed on a wood frame with 45° tilt angle so that the panel surface is normal to the irradiation. A pyranometer is used to measure and calibrate the solar irradiation. A mass flow meter is used to control the cooling water flow rate. The experimental data is collected with the data acquisition system. The whole system testing set up is shown in Fig. 2.

The performance of the solar panels are characterized in the following way: The solar panels are put in the solar room under different irradiations of 850 and 1100 W/m^2. Before the water flow starts, the solar panel surface temperature is automatically measured with an interval of 2 s until the panel reaches a stabilized

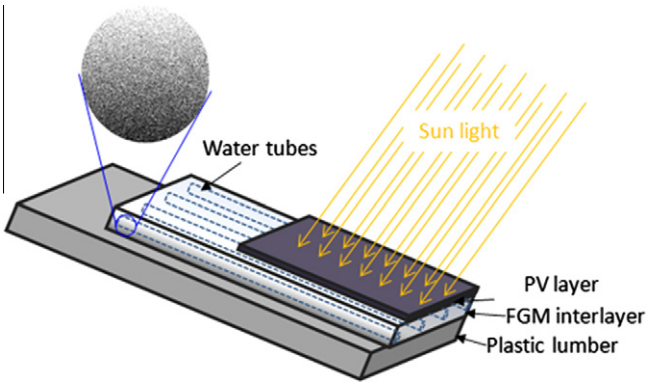

Fig. 1. Schematic illustration of the hybrid solar roofing panel prototype.

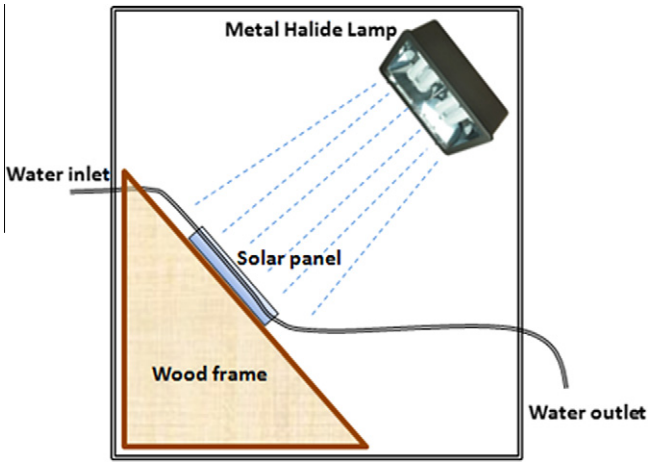

Fig. 2. Solar panel testing setup.

temperature. Then the water flow is introduced with the inlet water temperature at 20 °C. The flow rate is controlled by the mass flow meter at 33 and 66 ml/min for the irradiations of 850 and 1100 W/m^2, respectively. These water flow rates are determined by some trial-error tests so that the panel can be effectively cooled and the outlet water temperature keeps in a range between 32–34 °C. The irradiation levels are chosen to cover a small range around the AM1.5 (1000 W/m^2) condition. The PV cell and water temperatures are recorded continuously until the panel temperature stabilizes again.

3. Results and discussion

3.1. Irradiation space uniformity

During the tests, we use a metal halide lamp to simulate solar irradiation. The space uniformity of the irradiation is examined through 25 point measurement on the panel surface where is equally divided into 25 square areas. The 25 measuring points are uniformly distributed in the 25 square areas. Two different irradiation settings of 850 and 1100 W/m^2 are tested. The two dimensional irradiation contour maps are shown in Fig. 3. Irradiation maps are approximately symmetric within the panel with respect to the center point which receives the highest irradiations. It is reasonable as the panel surface is normal to the irradiation with the center aligned to the lamp. The coefficients of variation of the 25 point measurements are 2.9% and 3.3% for the irradiation of 850 and 1100 W/m^2, respectively.

3.2. Temperature distribution

Seven thermal couples are attached on the surface of the solar panel to evaluate the temperature distribution, as shown in Fig. 4, which also indicates the direction of water flow along the water tube by the arrows. For the data analysis conveniences, the sensor point number sequence follows the water flow direction. The eighth thermal couple is attached in the outlet water tube to test the outlet water temperature.

Fig. 5(a) shows the equilibrium temperature of the 8 points without and with water flow of 33 ml/min under the irradiation of 850 W/m^2, and Fig. 5(b) without and with water flow of 66 ml/min under the irradiation of 1100 W/m^2. It can be seen that even the irradiation map has the center high pattern, most region of solar panel still can be uniformly heated up, as the variation of the high equilibrium temperatures among the 7 points is within

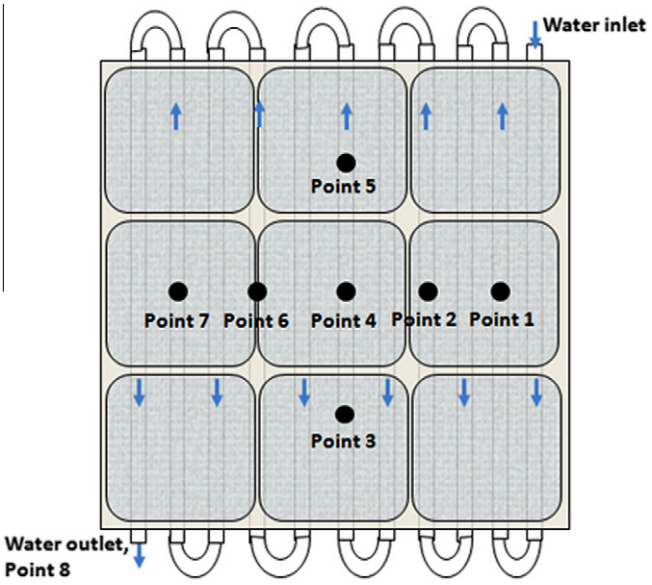

Fig. 4. Position of thermal couples and water flow direction.

±2 °C. With the water flow introduced, the temperatures of the 7 points monotonically increase with the point number sequence. As the higher the point number, the more thermal energy the water absorbed, and the less the cool effect. Fig. 6 shows the temperature variation with time at two different irradiations and water flow conditions. Before the water flow starts, the solar panel surface temperatures increase fast with time and then gradually saturate at around 50 and 55 °C at the time around 7700–8100 s for the irradiation of 850 and 1100 W/m^2, respectively. With the water flow introduced, the temperatures sharply dropped and then stabilized at around 32–38 °C. The outlet water temperature is around 32–34 °C. These results show that water tubes integrated with FGM layers can effectively cool the PV cells.

3.3. Finite element simulation

3.3.1. FEM and multilayer discretization

A commercial software package ABAQUS is used to simulate heat transfer across the solar panel. The model and grid generation of solar panel is shown in Fig. 7. The panel is discretized into eight layers in vertical direction including PV cells, thermal conductive

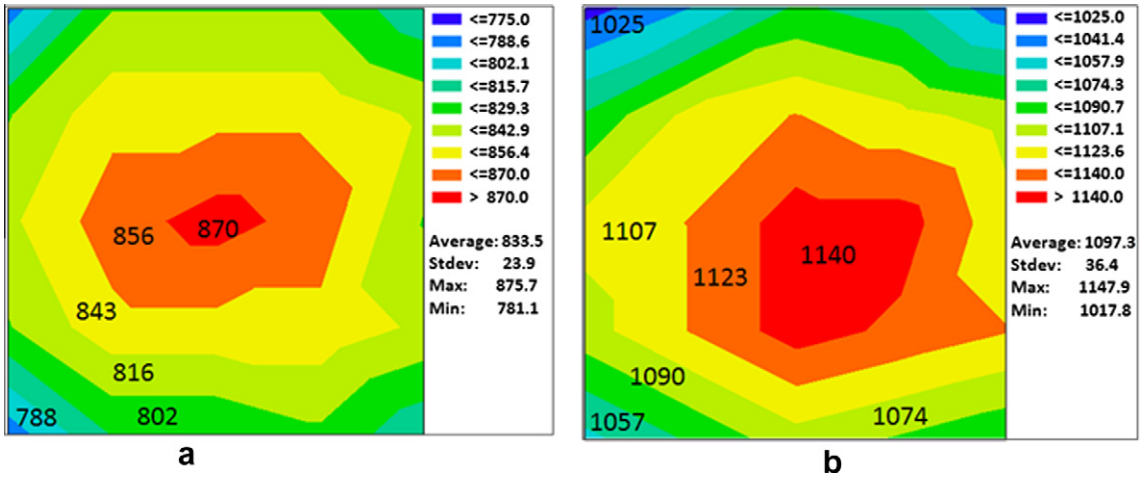

Fig. 3. Contour map of the solar irradiation on the panel surface for (a) 850 W/m^2 and (b) 1100W/m^2.

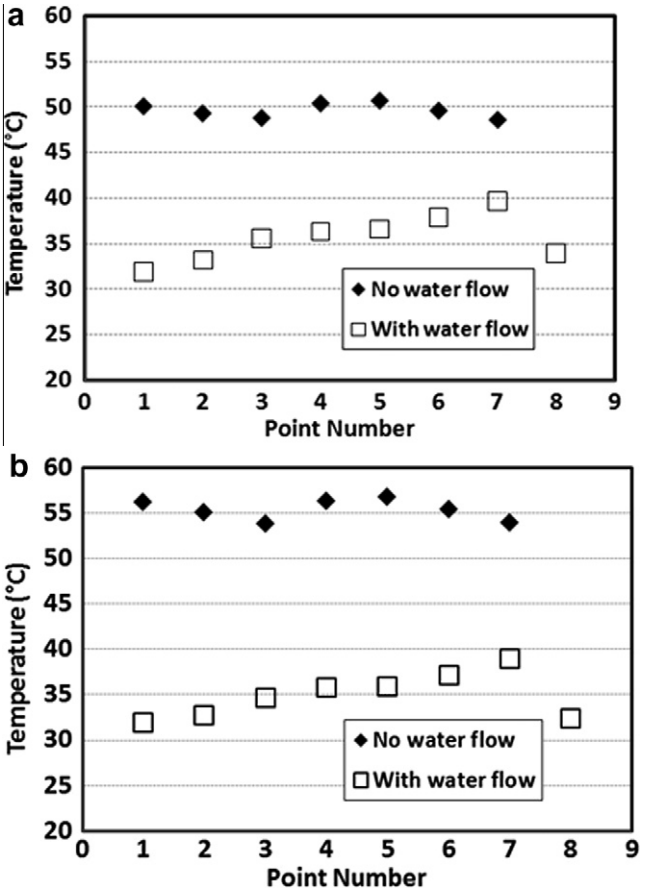

Fig. 5. Equilibrium temperatures of each point at conditions of (a) irritation: 850 W/m^2, water flow rate: 33 ml/min, (b) irritation: 1100 W/m^2, water flow rate: 66 ml/min.

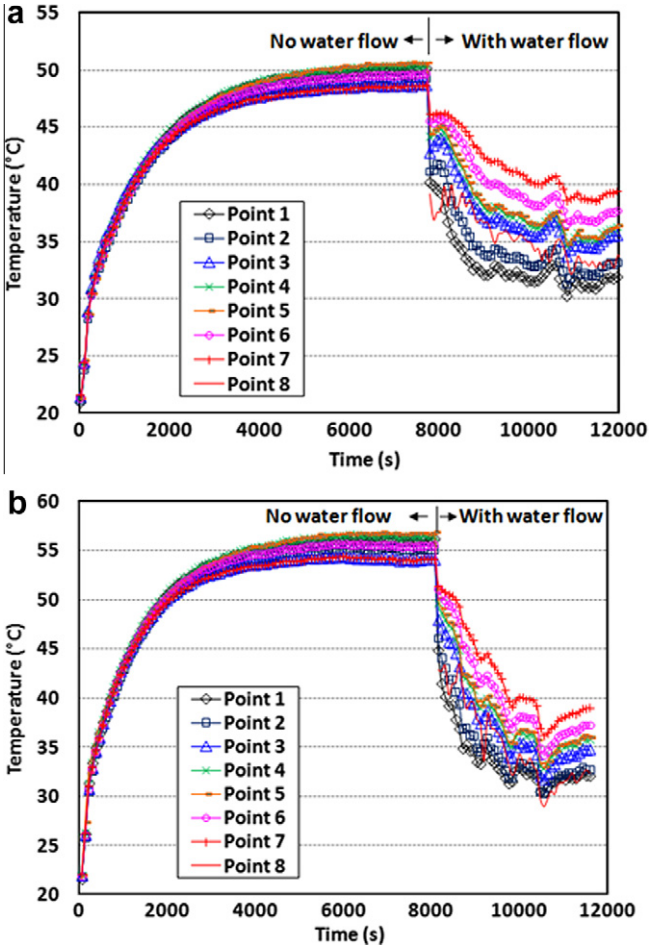

Fig. 6. Temperature variation with time diagram for (a) irritation: 850 W/m^2, water flow rate: 33 ml/min, (b) irritation: 1100 W/m^2, water flow rate: 66 ml/min.

paste, and six FGM layers with gradient variation of percentage of HDPE and aluminum. Within layer 4 and 5, there are 11 water tubes uniformly distributed. The thickness of copper tube is 1 mm and inner diameter is 4 mm. More grids are generated around tube area for better accuracy due to the curvature of water tube and fluid heat transfer characteristics.

3.3.2. Material specification

Within each FGM layer, material is assumed to be homogeneous, and the effective thermal conductivity can be calculated based on following equation [19].

$$\bar{k} = k_B \frac{\phi\alpha\left[1+\frac{\phi\beta^2}{4}\right]+(1-\phi)}{\phi\frac{k_B}{k_A}\alpha\left[1+\frac{\phi\beta^2}{4}\right]+(1-\phi)} \tag{1}$$

where k_A, k_s is the thermal conductivity of particle phase A and matrix B, respectively, which stand for two constitution particulate materials for the FGM layer, e. g. the Al and HDPE powders. ϕ is volume fraction of particle phase A, and α, β are defined as [19]

$$\alpha = \frac{3k_A}{k_A+2k_B}, \beta = \frac{k_A-k_B}{k_A+2k_B} \tag{2}$$

By using the thermal conductivity values of 238 and 0.26 W/m K for Al and HDPE, respectively, the effective thermal conductivity of HDPE/Al matrix with different volume fraction can be calculated. Table 1 lists the dimension and properties of each layer and material that are used in the finite element simulation.

3.3.3. Thermal energy circulation

The total input solar energy E_{in} is simulated using the numerical integration of the 25 point irradiation value shown in Fig. 3. A one dimensional thermal conduction model is used to simulate the heat transfer between and within each layer. The radiation and convection heat loss can be calculated as:

$$E_{rod} = \epsilon \cdot s \cdot (T_{pv}^4 - T_{am}^4) \tag{3}$$

$$E_{con} = h_c \cdot (T_{pv} - T_{am}) \tag{4}$$

where ε, s, h_c, T_{pv} and T_{am} are the average surface emissivity of silicon ~0.6, Stefan–Boltzmann Constant ~5.67 × 10^{-8} W/m^2 K^4, convection coefficient of air ~5 W/m^2 K, panel surface temperature and ambient temperature, respectively [20,21]. The solar room ambient temperature, T_{am}, is also continuously recorded with the range from 25 to 35 °C. A forced convention model is used to describe the heat transfer between the water and the FGM layers. The Nusselt number is defined as [22]

$$Nu = \frac{h_w D}{k} \tag{5}$$

where h_w is convection heat transfer coefficient of water, D is water tube diameter, and k is thermal conductivity of water, which is approximately 0.58 W/m K. Normally, for fully developed pipe flow with uniform wall heat flux, Nusselt number is given by

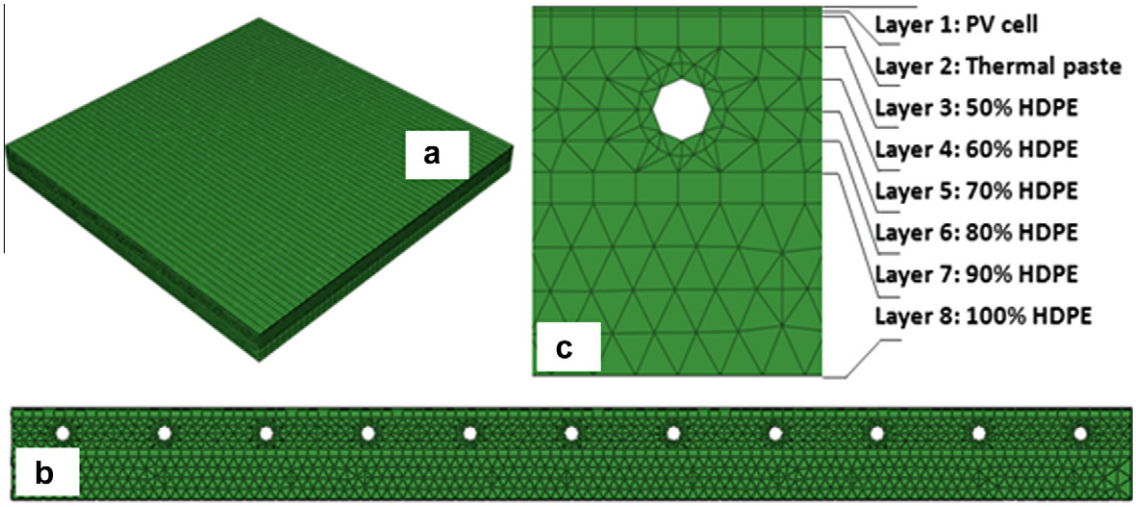

Fig. 7. FEM and grid generation for (a) whole of solar Panel, (b) close up of the cross section, and (c) close up of a water tube.

Table 1
Thickness and properties of each material used in FEM simulation.

Layer/material	Thickness (mm)	Density g/cm^3	Specific heat J/g K	Thermal conductivity W/m K
1, PV cell (Si)	0.27	2.33	0.7	130
2, Silicone thermal paste	0.30	2.6	0.7	1.9
3, 50% HDPE	2	1.83	1.58	1.13
4, 60% HDPE	2	1.65	1.74	0.83
5, 70% HDPE	2	1.48	1.85	0.62
6, 80% HDPE	2	1.30	1.98	0.46
7, 90% HDPE	2	1.13	2.12	0.35
8, 100% HDPE	13	0.95	2.25	0.26
Copper tube	1	8.94	0.39	401
Water	–	1	4.18	0.58

$Nu = 48/11 = 4.36$ [22]. For this model, D is the copper pipe diameter of ~4 mm, so the heat convection transfer coefficient of water is

$$h_w = \frac{Nu \cdot k}{D} = 632.2 \frac{W}{m^2} \cdot K \tag{6}$$

For simplicity, we assume the water temperature increases linearly along the water flow path, which can be effectively justified by the data in Fig. 5. Once we know the temperatures of inlet water and outlet water at one time, the temperature distribution of water flow along the full path within the FGM layer can be approximated for heat transfer simulation in the FEM.

3.3.4. Simulation results

Fig. 8 shows the equilibrium temperature space distribution in the panel at the condition of the irradiation at 1100 W/m^2 and the water flow rate at 66 ml/min. The red[1] color and blue color stand for high and low temperatures, respectively. Before the water flow starts, the whole panel surface is uniformly heated up, as depicted in Fig. 8(a). When the water flow was introduced, the overall panel surface temperature decreased and linearly distributed from the inlet to outlet position, as shown in Fig. 8(b), which is consistent with the experimental observations in Fig. 5, where the temperatures of point 1–7 monotonically increase with the point number.

The temperature variation with time of the 7 points on the panel are also simulated and compared to the experimental results.

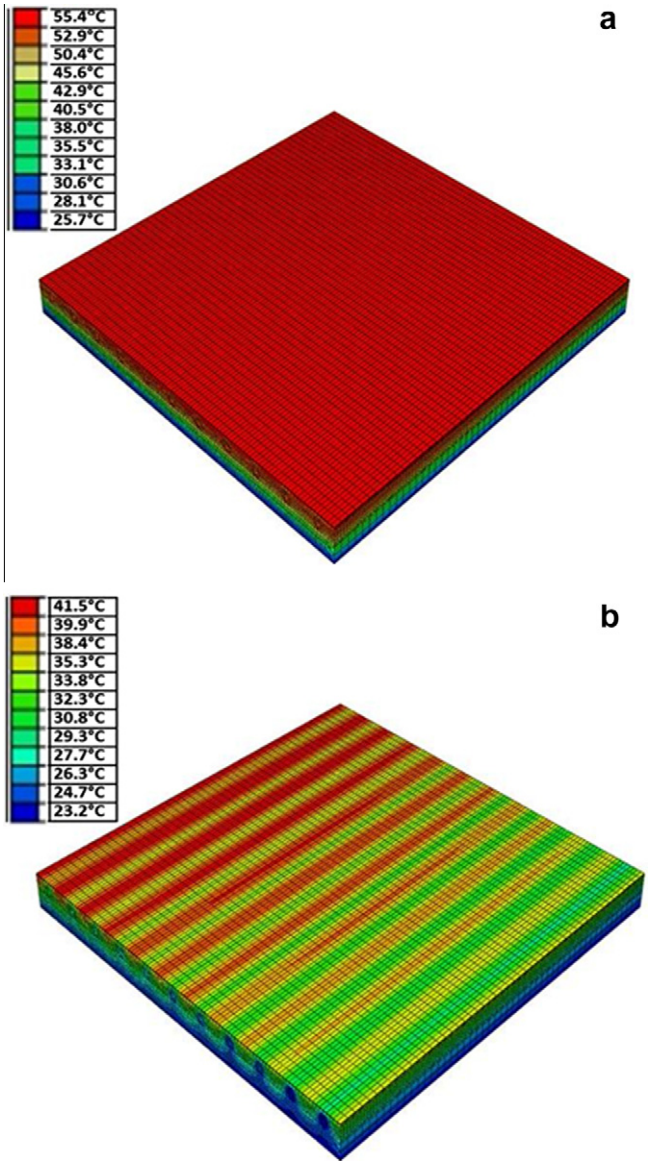

Fig. 8. Temperature space distributions of the panel at (a) 1100 W/m^2 irradiation without water flow, (b) 1100 W/m^2 irradiation with water flow of 66 ml/min.

[1] For interpretation of color in Fig. 8, the reader is referred to the web version of this article.

As the data profiles of both experiment and simulation for the 7 points are practically the same, only the results of point 4 are shown in Fig. 9. Basically, the FEM simulation results well fit to the experiments. There is a gap (8% mismatch) between the FEM simulations and experiment data at the initial stage of the temperature increment. This can probably be related to the non-stability of the solar room conditions, such as the air circulation or solar irradiation power, which may contribute to the lower surface temperature of the solar panel compared to simulations. At the equilibrium conditions without water flow, the FEM simulations have good agreement with the experiment data with less than 2.5% difference. At the temperature falling region after the water flow introduced, the temperature fluctuation of the experiment data is due to the variations of the water flow rate, which is difficult to control at low flow rate. Better fittings in Fig. 9(b) can be achieved at high water flow rate, e.g. 66 ml/min, which normally is more stable compared to 33 ml/min.

3.4. Energy efficiency analysis

From the simulation and experimental data, it is found that FGM based water tubes can effectively reduce the panel temperature. For the case of 1100 W/m^2 irradiation with 66 ml/min water flow, the panel temperature can be reduced from 55 to 35 °C (average from 32 to 38 °C). The single crystalline Si solar cell efficiency is 13 % at room temperature and normally decreases with temperature. Based on the crystalline Si cell efficiency temperature coefficient of −0.54 %/°C characterized in another work [23], the efficiency of the PV cell will downgrade to 10.8% at 55 °C and recover to 12.3% at 35 °C with the FGM cooling function. So that the PV cell performance can keep around 95% of that at room temperature even under 1100 W/m^2 irradiation. Using the 25 point irradiation value in Fig. 3, the total input solar energy E_{in} on the panel can be numerically calculated to be 93.9 W and electric energy generated from PV cell is $E_{pv} = E_{in} \times 12.3\% = 11.5$ W. In addition, the thermal energy collected by water per second is around $E_{water} = m_{water} \times C_{water} \times T_{water} = 1.1\ g \times 4.18\ W/g\ °C \times 12\ °C = 55.2$ W. (The outlet water temperature in around 32 °C based on Fig. 6(b)). Thus the overall efficiency of the panel is $\eta = (E_{water} + E_{pv})/E_{in} = (55.2 + 11.5)/93.9 = 71\%$, which are very promising results compared to those of traditional PV thermal hybrid solar panels. The energy efficiency analysis and comparisons with traditional panels are summarized in Table 2.

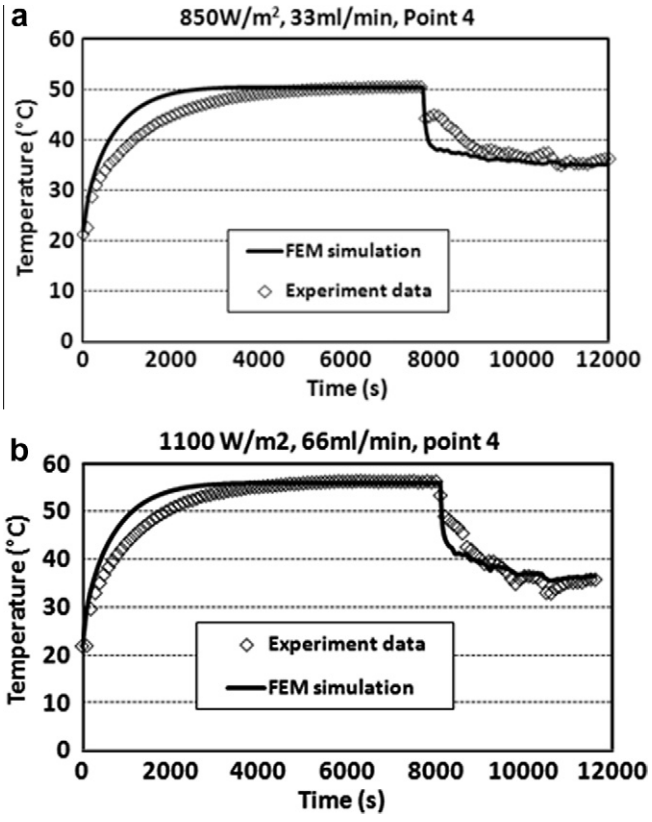

Fig. 9. FEM simulation and experimental data of the temperature distribution under (a) 850 W/m^2 irradiation and 33 ml/min water flow rate (point 4), and (b) 1100 W/m^2 irradiation and 66 ml/min water flow rate (point 4).

Table 2
Energy and efficiency summary and comparisons.

Panel type		Electric energy (W)	Thermal energy (W)	Efficiency (%)
FGM based hybrid solar panel	Without water	10.1	0	10.8
	With water	11.5	55.2	71.0
Traditional liquid-type PV thermal hybrid solar panel (Ref.)				53–68.2 [24]

4. Conclusions

A novel solar panel integrated with photovoltaic cells and water tubes embedded in functionally graded material (FGM) is fabricated. The FGM layer can effectively transfer heat from the PV cells to water tubes and prevent heat loss to the substrate. The hybrid solar panel exhibits promising performance with PV cells working at relatively low temperatures. Considering electricity and thermal energy collection, the overall panel efficiency is around 71%, which compares favorably with those of traditional PV thermal hybrid solar panels. A finite element model was successfully built to simulate the heat transfer characteristics in the hybrid solar panel prototype and the simulation results are consistent with the experimental data. It provides a general approach for future FGM based solar panel design and optimization.

Acknowledgements

This work is sponsored by the National Science Foundation CMMI 0954717 and Department of Energy STTR DE-SC0003347, whose support is gratefully acknowledged. The authors are also grateful to Liming Li and Adrian Brügger, managers of Carleton Laboratory, for their strong support on the solar panel fabrication and testing. In addition, students Pablo Presto-Munoz, Michael Lackey, Alaa Saleh, and Steven Wong participated in the fabrication of hybrid solar panel prototypes, Michael Shields participated in the test design, Greg Kelly from Weidlinger Associates Inc. and Jacques Garant from HLW International participated in the water tube connection. The contribution from all of them is highly appreciated.

References

[1] R. Levy, Solar energy conversion can be small-scale and low-tech, Phys. Today 60 (2007) 2–14.
[2] W. Shockley, H.J. Queisser, Detailed balance limit of efficiency of P–N junction solar cells, J. Appl. Phys. 32 (1961) 510–519.
[3] A.J. Nozik, Spectroscopy and hot electron relaxation dynamics in semiconductor quantum wells and quantum dots, Annu. Rev. Phys. Chem. 52 (2001) 193–231.
[4] S. Odeh, M. Behnia, Improving photovoltaic module efficiency using water cooling, Heat Transfer Eng. 30 (2009) 499–505.
[5] R.J. Kaplar et al., Deep levels in p- and n-type In GaAsN for high-efficiency multi-junction III-V solar cells, Sol. Energy Mater. Sol. Cells 69 (2001) 85–91.
[6] T. Trupke et al., Improving solar cell efficiencies by down-conversion of high-energy photons, J. Appl. Phys. 92 (1) (2002) 1668–1674.

[7] R.D. Schaller, V.I. Klimov, High efficiency carrier multiplication in PbSe nanocrystals: Implications for solar energy conversion, Phys. Rev. Lett. 92 (2004) 186601-1–186601-4.
[8] R.T. Ross, A.J. Nozik, Efficiency of hot-carrier solar-energy converters, J. Appl. Phys. 53 (1982) 3813–3818.
[9] D. Vincenzi et al., Concentrating PV system based on spectral separation of solar radiation, Phys. Status Solidi a Appl. Mater. Sci. 206 (2009) 375–378.
[10] R.H. Crawford et al., Life-cycle energy analysis of building integrated photovoltaic systems (BiPVs) with heat recovery unit, Renewable Sustainable Energy Rev. 10 (2006) 559–575.
[11] H.A. Zondag, Flat-plate PV-Thermal collectors and systems: A review, Renewable Sustainable Energy Rev. 12 (2008) 891–959.
[12] Y. Vorobiev et al., Thermal-photovoltaic solar hybrid system for efficient solar energy conversion, Sol. Energy 80 (2006) 170–176.
[13] D. Kraemer et al., Photovoltaic-thermoelectric hybrid systems: a general optimization methodology, Appl. Phys. Lett. 92 (16) (2008) 243503-1–243503-3. 243503-1-3.
[14] H.M. Yin, Integrated functionally graded solar roofing panel for PV and heat utilization, US Patent: 61/178,721, 61/220,082, 2009.
[15] Y. Miyamoto, W.A. Kaysser, B.H. Rabin, A. Kawasaki, R.G. Ford, Functionally Graded Materials: Design, Processing and Applications, Kluwer Academic Publishers, Dordrecht, 1999.
[16] H.M. Yin et al., Heat flux field for one spherical inhomogeneity embedded in a functionally graded material matrix, Int. J. Heat Mass Transfer 51 (2008) 3018–3024.
[17] H.M. Yin et al., Micromechanics-based thermoelastic model for functionally graded particulate materials with particle interactions, J. Mech. Phys. Solids 55 (2007) 132–160.
[18] H.M. Yin et al., Micromechanics-based elastic model for functionally graded materials with particle interactions, Acta Mater. 52 (2004) 3535–3543.
[19] G.H.P.H.M. Yin, W.G. Buttlar, L.Z. Sun, Effective thermal conductivity of two-phase functionally graded particulate composites, J. Appl. Phys. 98 (2005). 063704-1-9.
[20] S. Wielder, An Introduction to Solar Energy for Scientist and Engineer, John Willy & Sons, 1982.
[21] B. Sopori et al., Calculation of emissivity of Si wafers, J. Elec. Mater. 28 (1999) 1385–1389.
[22] A. Bejan, Convecion Heat Transfer, third ed., John Wiley & Sons, inc., 2004.
[23] D.J. Yang, H.M. Yin, Energy conversion efficiency of a novel hybrid solar system for photovoltaic, thermoelectric, and heat utilization, IEEE Trans. Energy Convers. 26 (2011) 662–670.
[24] T.T. Chow, A review on photovoltaic/thermal hybrid solar technology, Appl. Energy 87 (10) (2010) 365–379.